

# Enhancing the Generalization of Flood Susceptibility Models: A Leakage-Aware Ensemble Framework for Deltaic Landscapes

Shafiq Mahmud<sup>1</sup>, Golam Murad<sup>2</sup>, Md. Aftabur Rahman<sup>3\*</sup>

<sup>1</sup>Undergraduate Student, Department of Urban and Regional Planning, Chittagong University of Engineering & Technology, Chattogram-4349, Bangladesh, Email: [u2105051@student.cuet.ac.bd](mailto:u2105051@student.cuet.ac.bd)

<sup>2</sup>Graduate, Department of Civil Engineering, Chittagong University of Engineering & Technology, Chattogram-4349, Bangladesh, Email: [u1901087@student.cuet.ac.bd](mailto:u1901087@student.cuet.ac.bd)

<sup>3</sup>Professor, Department of Civil Engineering, Chittagong University of Engineering & Technology, Chattogram-4349, Bangladesh, Email: [maftabur@cuet.ac.bd](mailto:maftabur@cuet.ac.bd)

\*Corresponding Author: Md. Aftabur Rahman

## Abstract

Flood susceptibility mapping (FSM) is a cornerstone of disaster risk reduction in low-lying deltaic regions; however, conventional machine learning (ML) applications frequently suffer from spatial data leakage, resulting in inflated performance metrics and unreliable hazard predictions. To address this critical methodological shortcoming, this study develops a robust, leakage-aware ML framework for FSM in the highly vulnerable Greater Noakhali region of Bangladesh. Utilizing a flood inventory derived from Sentinel-1 SAR imagery of the catastrophic August 2024 event, we integrated twelve spatially explicit conditioning factors representing topographic, hydrological, and anthropogenic drivers. To ensure true model generalization and mitigate the effects of spatial autocorrelation, eight ensemble algorithms were evaluated using a rigorous 10-fold blocked spatial cross-validation strategy. The spatially constrained evaluation provided realistic performance estimates, in contrast to the overly optimistic ROC-AUC values typical of conventional random splits, with Random Forest demonstrating the highest generalization capability (ROC-AUC = 0.627) and XGBoost achieving the optimal balance between precision and recall (F1 = 0.451). Furthermore, SHAP (SHapley Additive exPlanations) analysis of the ensemble models identified land use, vegetation density (NDVI), and drainage density as the primary physical drivers of flood susceptibility in this coastal tract. By demonstrating that spatially robust validation is essential for credible geospatial AI, the resulting maps identify critical high-risk zones along the Meghna estuary and provide a physically plausible, operationally relevant tool for regional disaster management.

**Keywords:** Flood susceptibility mapping, Spatial data leakage, Spatial cross-validation, Machine learning, Random Forest, XGBoost, SHAP analysis, Remote sensing, Bangladesh, Noakhali region.

## Introduction

Floods are one of the most common and damaging natural hazards globally shaped by overflowing water standing, caused as an effect of more volume of water to rest due to a lot of rain, river flooding storm surges or dam failure (Shampa et al. 2025). These events disrupt ecosystems, damage infrastructure, and endanger human lives predicting significant economic losses along with long term socioeconomic impacts (Yao et al. 2026).

Among flood-prone countries, Bangladesh stands out due to its unique geographical and hydrological setting (Paszkowski et al. 2025). The country lies at the meeting point of the Ganges, Brahmaputra and Meghna river systems, which channel large upstream flows into the

44 seaward direction during monsoon seasons (Paszkowski et al. 2025). This environment, when  
45 taken together with its predominantly low-lying alluvial floodplains and elevation in relation  
46 to potential coastal storm surges from the Bay of Bengal, renders wide areas of the country  
47 vulnerable to frequent flooding (Elahi et al. 2025).

48 The southeastern coastal belt of Bangladesh, especially Greater Noakhali (Noakhali,  
49 Lakshmipur and Feni Districts) is one of the most vulnerable flood-prone zones in Bangladesh  
50 (Sarker and Jahan 2026). Flood vulnerability is, however, exacerbated still further due to the  
51 region's low elevation, flat topography and dense drainage network as well as strong tidal forces  
52 (Piya et al. 2026). Previous catastrophic events such as August 2024 flash flood in this region,  
53 which affected more than 550,000 further underlines the need for solidifying a unique  
54 methodology with proper flood assessment frameworks (Huang 2025).

55 Flood susceptibility mapping (FSM) is a crucial disaster risk reduction tool that assists in land-  
56 use planning, early warning systems, and climate adaptation strategies (Rashid et al. 2026).  
57 Existing standard flood modelling approaches are physically based hydrodynamic models;  
58 however, their high computational requirement and data-intensive nature limit the  
59 applicability, especially in data-scarce environments (Aniramu et al. 2026). On the other hand,  
60 machine learning (ML) techniques can be a flexible and fast alternative that has great potential  
61 for modelling complex nonlinear relationships between flood occurrence and conditioning  
62 factors such as topography, hydrology, land use, and climate variables (Ganiyu et al. 2026).  
63 Ensemble-based approaches such as Random Forest, XGBoost and LightGBM have been  
64 reported to be highly accurate across different geographical locations (Rahman and Yasuhara  
65 2026).

66 Yet, a key methodological issue for geospatial ML applications relates to spatial data leakage  
67 which is caused by spatial autocorrelation between samples (Grekousis 2025). Popular train-  
68 test splits often introduce spatial proximity between samples that nonetheless appear in both  
69 datasets, giving rise to biased and overly optimistic performance estimates which are contrary  
70 to what a true generalization of the model will yield (Li et al. 2023). This problem is most  
71 evident in low-lying flood-sensitive areas such as Bangladesh, where spatial dependency is  
72 high yet neglected (Alif et al. 2025).

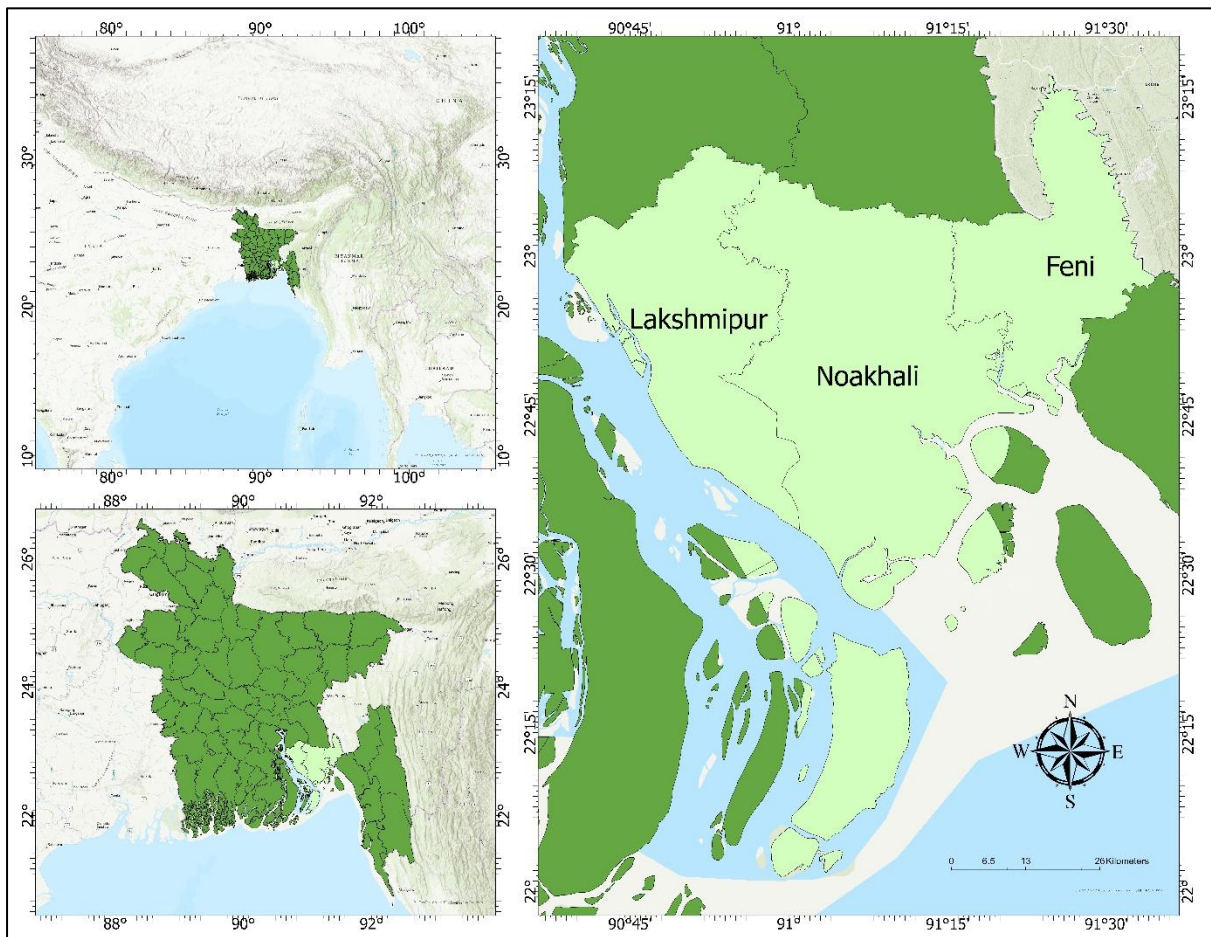
73 These limitations have been addressed by spatially explicit validation strategies (i.e. spatial  
74 cross-validation, block-based holdout) that restrict geographic proximity of data for training  
75 and evaluation to obtain more realistic estimates of model performance (Islam et al. 2026).  
76 These approaches are effective yet not commonly applied in deltaic environments where  
77 reproducible and reliable modeling frameworks are urgently needed (Nnam et al. 2026).

78 In this scenario, the current study proposed a leakage aware flood susceptibility mapping  
79 framework using classical machine learning techniques under strict spatial holdout design for  
80 Greater Noakhali area (Tella et al. 2026). A systematic evaluation of eight popular models,  
81 Decision Tree, Random Forest, Extra Trees, AdaBoost, Gradient Boosting,  
82 HistGradientBoosting, XGBoost and LightGBM, is conducted using a block-based spatial  
83 partitioning scheme (Rahimi et al. 2026). Flood inventory is obtained from Sentinel-1 and  
84 conditioning factors are constructed with terrain, hydrological, and land-use datasets (Asrade  
85 et al. 2026). A consistent preprocessing pipeline is used, with one-hot-encoding of land  
86 use/land cover, cyclic transformation of aspect variables, and median imputation with missing-  
87 indicator features to maintain reproducibility and prevent feature-level leakage (Elmotawakkil  
88 et al. 2025). Additionally, SHAP analysis is used to explain the predictions of the model and  
89 measure how important some conditioning factors are (Gupta et al. 2026).

90 The objective of this study is to assess the performance of classical machine learning models  
91 using strict spatial validation, create a reproducible geospatial modeling workflow free from  
92 leakage and evaluate tree-based ensemble techniques for flood susceptibility mapping. It also  
93 aims to produce realistic susceptibility maps for regional planning and disaster risk  
94 management. This research that focuses on computation efficient interpretable models places  
95 an emphasis on leakage aware evaluation and shows moderate performance metrics to be the  
96 most credible foundations for assessment of regularly occurring flood susceptibility in coastal  
97 Bangladesh.

## 98 Study Area

99 The study was performed at the Greater Noakhali region, located in the southeastern coastal  
100 zone of Bangladesh. Three administrative districts - Noakhali, Lakshmipur and Feni constitute  
101 this region. Geographically, the study area is defined roughly between 22°30'N to 23°15'N  
102 latitude and 90°45'E to 91°45'E longitude, covering one of the low-lying deltaic landscapes  
103 bordering northern Bay of Bengal.



104  
105

*Figure 1: Study Area Map*

106 This region is almost flat and low elevated geomorphology with all the areas lying in 0–5 m  
107 above mean sea level is vulnerable to inundation (Sorna et al. 2025). Majority of the landform  
108 are recent alluvial deposits, formed through dynamic interaction between Meghna River system  
109 and coastal sediment transfer (Ali et al. 2025). The region belongs to the Ganges–  
110 Brahmaputra–Meghna (GBM) delta, with perpetual geomorphological evolution characterized

111 by ongoing pro-cesses of accretion and erosion that further modulate flood dynamics (Khan  
112 2021).

113 The study area is a highly dense, interconnected system of rivers tidal channels and canals  
114 (locally called khals) with the western and southern edges bounded by the Meghna estuar  
115 (Valentine and Wilson 2023). I think it is this intertwined drainage which makes a stage of  
116 flood regime both from the upstream and downstream tidal propagation (Elahi et al. 2025). As  
117 a result, the region is vulnerable to both fluvial flooding due to upstream discharge in times of  
118 high monsoon flow as well as tidal flooding and storm surges from the Bay of Bengal (Elahi  
119 et al. 2025).

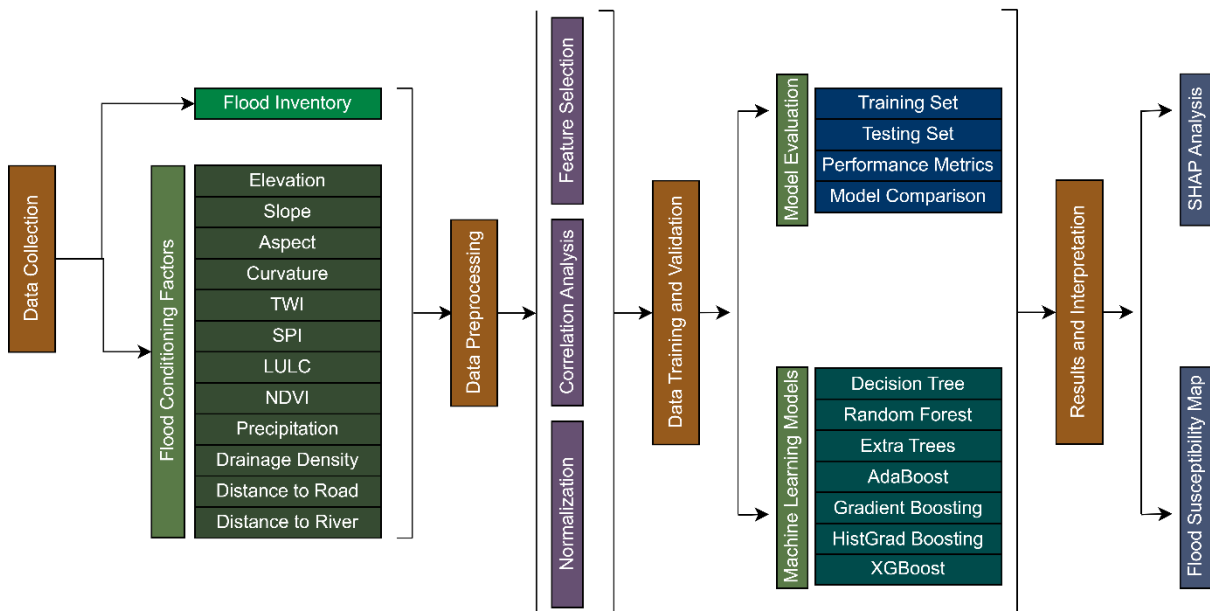
120 The region is characterized by tropical monsoon climate with most annual precipitation  
121 occurring between June and September (Das et al. 2021). Heavy rainfall during this period  
122 often overlaps with high river discharge and tidal phase, thus posing additional flood risk.  
123 Besides, temporality extreme flooding incidents are established to be associated with cyclonic  
124 activities in the Bay of Bengal, especially in coastal and estuarial regions (Dutta et al. 2025).

125 Over the last decades, accelerated agricultural intensification and land-use changes such as  
126 more settlements, urbanization, and infrastructure have modified the alteration of natural  
127 hydrological response within that area (Dixit et al. 2024). These modifications have diminished  
128 the natural drainage capability and have amplified the surface runoff, making the region more  
129 flood sensitive.

## 130 Methodology

131 The overall workflow of this study follows a structured, leakage-aware machine learning  
132 pipeline for flood susceptibility mapping, consisting of data collection, preprocessing, feature  
133 analysis, model development, evaluation, and interpretation.

134



135

136

Figure 2: Methodology Flowchart

137

138 The data collection step consists of a flood inventory dataset and many conditioning factors  
139 compiled from remote sensing and geospatial sources. The flood inventory obtained from

140 Sentinel-1 SAR Imagery and twelve factors, i.e. elevation, slope, aspect, curvature,  
141 Topographic Wetness Index (TWI), Stream Power Index (SPI), Land use Land cover (LULC),  
142 NDVI, Precipitation, Drainage density distance to roads and Distance to rivers used as  
143 topographic-hydrological-environmental-anthropogenic influences were all prepared in a GIS  
144 environment.

145 After data acquisition, all variables are preprocessed to ensure they are compatible with the  
146 model. This involves missing value imputation, categorical variable encoding (LULC), cyclical  
147 feature transformations (aspect), and continuous variable normalization. Operations of this  
148 manner are done only on the training data to avoid data leakage.

149 In the next step, feature analysis via correlation and statistical metrics is performed to identify  
150 redundant or highly collinear variables that would enhance model robustness, focus on key  
151 predictors of interest, improve interpretability whilst mitigating overfitting.

152 Next building dataset dividing in a train and test subset with a spatially aware strategy subject  
153 to avoid spatial autocorrelation. Metrics include using ROC-AUC, precision, recall and F1  
154 score to evaluate models against testing set after training on the training set.

155 Multiple machine learning algorithms are used in the model development stage such as  
156 Decision Tree, Random Forest, Extra Trees, and Boosting methods like AdaBoost, Gradient  
157 Boosting, HistGradient Boosting and XGBoost that follow a similar pipeline to enable standard  
158 comparison amongst different models.

159 Based on the evaluation description and predictive stability, the model with the best  
160 performance is selected. SHAP (SHapley Additive exPlanations) analysis is then performed to  
161 interpret model behavior and deduce the contribution of each conditioning factor. Finally, a  
162 final model is applied to produce the flood susceptibility map.

## 163 **Flood Inventory and SAR Imagery**

164 A consistent flood inventory is an essential component of supervised flood susceptibility  
165 modelling (Murad et al. 2025). In this study, the flood inventory was prepared based on the  
166 August 2024 flood event which inundated most of the districts such as Noakhali, Lakshmipur  
167 and Feni in Greater Noakhali region.

168 Land flood area contours using multi-temporal Sentinel-1 Synthetic Aperture Radar (SAR)  
169 images is widely used in tropical and monsoon-dominated countries for its all-day, all-weather  
170 imaging ability (Hussain et al. 2023). SAR, unlike optical sensors, is able to penetrate cloud  
171 cover and therefore is notably useful for monitoring flood extent during high rainfall events  
172 (Shatov et al. 2026).

173 Backscatter differences from pre- and post-event scattering coefficients were used to extract  
174 inundated areas from processed SAR images, where floodwater typically has a low backscatter  
175 signature due to specular reflection. This combined flood extent map was subsequently  
176 sampled at point locations representing flood (1) and non-flood (0) classes.

177 After filtering data with missing values in target, we would have 14,988 labeled samples  
178 collected. Out of these, 4,109 samples are related to floods having a positive class ratio of  
179 27.42%, and the remaining refers to non-flood conditions.

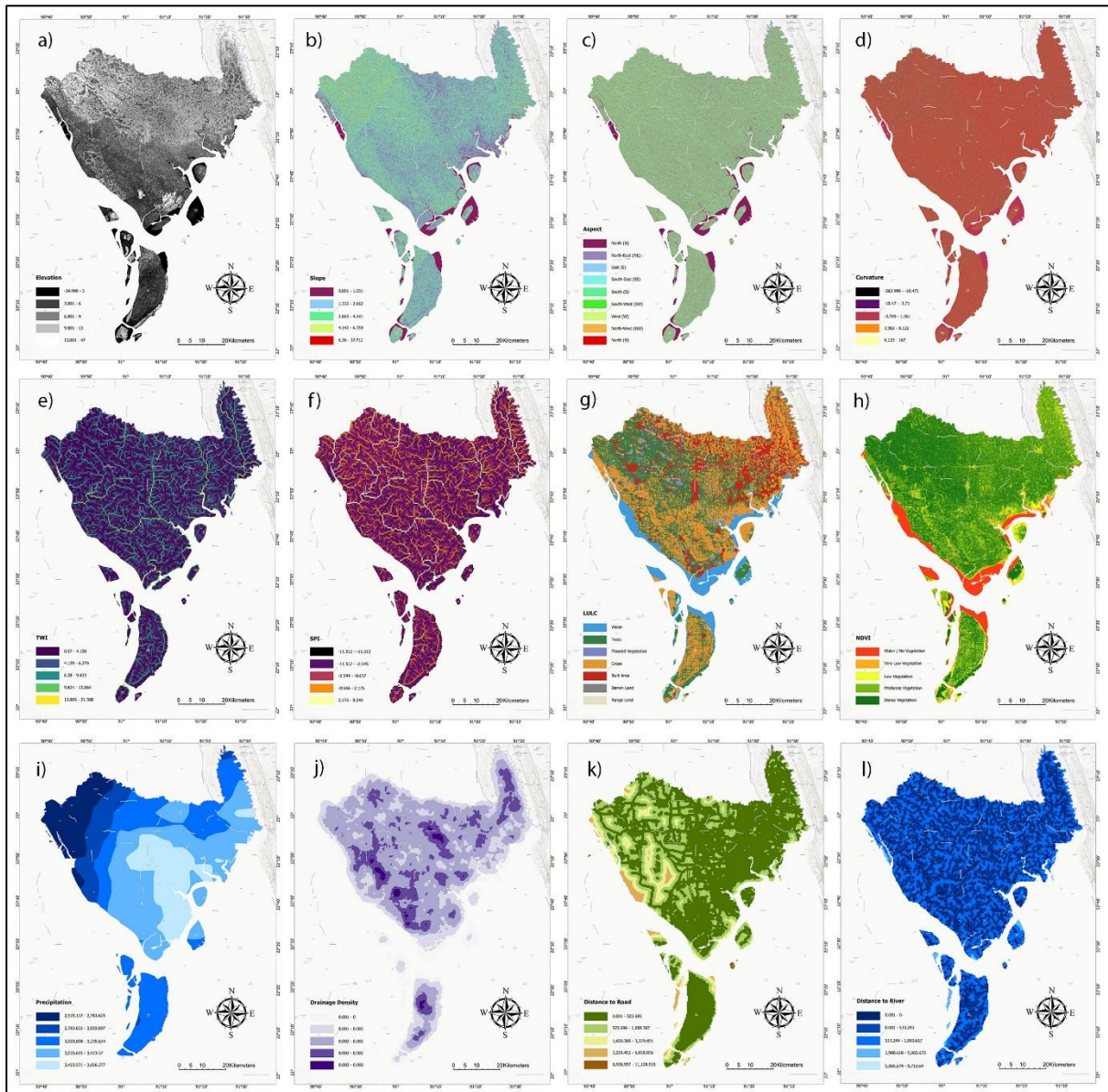
180 Spatially stratified random sampling generated non-flood samples defining various regions of  
181 the study area ensuring sufficient spatial coverage and minimizing bias. To prevent spatial  
182 duplication and clustering effect, special caution was spent to make sure each sample represents  
183 unique geography.

184 Such a flood inventory yields an ample and spatially balanced set of training and evaluation  
 185 data that can be used for training and evaluating machine learning models under strict  
 186 conditions of spatial validation.

187

## 188 Flood Conditioning Factors

189 Flood Event is a result of intricate topographic, hydrologic, climatic and anthropogenic  
 190 interactions (Dal Seno et al. 2024). Out of a total of twenty-five candidate variables, twelve  
 191 conditioning factors deemed useful based on their common use in flood susceptibility studies  
 192 and availability for the study area were selected out and grouped into three categories:



193

194 *Figure 3: Flood Conditioning Factors: a)Elevation, b)Slope, c)Aspect, d)Curvature, e)TWI, f)SPI, g)LULC,*  
 195 *h)NDVI, i)Precipitation, j)Drainage Density, k)Distance to Road, l)Distance to River.*

196

197

198

199 Hydrological Factors

200 Topographic Wetness Index (TWI): TWI is a measure of the spatial variability and potential  
201 accumulation of soil moisture (Murad et al. 2026). It is defined as:

$$TWI = \ln \left( \frac{A_s}{\tan \beta} \right) \quad 1$$

202

203

204 Stream Power Index (SPI): SPI is a surrogate variable for the erosive power of flowing water,  
205 directly computable from slope and flow accumulation (Ghasemian et al. 2022).

206 Drainage density: This indicates the total length of a stream unit area and its related areas (Das  
207 and Lepcha 2019).

208 Distance to River: The distance from rivers is an important measure of flood risk as the closer  
209 a location is to river channels, the higher the chances of flooding during peak discharge periods  
210 (Habumugisha et al. 2022).

211 Environmental and Anthropogenic Factors

212 Land Use/Land Cover (LULC): LULC affects infiltration, runoff and water retention. Urban  
213 or built-up areas often cause surface runoff to escalate, while active vegetated areas increase  
214 infiltration and reduce the risk of flooding (Dahim et al. 2023).

215 Distance to Road: Road infrastructure can also disturb natural drainage patterns and provide  
216 barriers to water flow (Abedin et al. 2020).

217 Normalized Difference Vegetation Index (NDVI): NDVI is a key representor of vegetation  
218 density and health. Infiltration and evapotranspiration are higher in areas with a higher NDVI,  
219 leading to reduced propensity for flooding (Ren et al. 2024).

220 Precipitation: Precipitation is a direct driver of flood events (Kumar et al. 2026). Spatial  
221 variability in rainfall intensity significantly influences flood occurrence (Kumar et al. 2026).

222

223

224

225

226

227

228

229

230

231

Table 1: Factors' Data Source and Resolution

Factor	Source of Data	Spatial Resolution (m)
Elevation	<a href="https://earthexplorer.usgs.gov/">https://earthexplorer.usgs.gov/</a> SRTM DEM	30 m × 30 m
Slope	<a href="https://earthexplorer.usgs.gov/">https://earthexplorer.usgs.gov/</a> Derived from SRTM DEM	30 m × 30 m
Aspect	<a href="https://earthexplorer.usgs.gov/">https://earthexplorer.usgs.gov/</a> Derived from SRTM DEM	30 m × 30 m
Curvature	<a href="https://earthexplorer.usgs.gov/">https://earthexplorer.usgs.gov/</a> Derived from SRTM DEM	30 m × 30 m
SPI	<a href="https://earthexplorer.usgs.gov/">https://earthexplorer.usgs.gov/</a> Derived from SRTM DEM	30 m × 30 m
TWI	<a href="https://earthexplorer.usgs.gov/">https://earthexplorer.usgs.gov/</a> Derived from SRTM DEM	30 m × 30 m
NDVI	<a href="https://earthexplorer.usgs.gov/">https://earthexplorer.usgs.gov/</a> Landsat 8 Level-2 Surface Reflectance	30 m × 30 m
LULC	<a href="https://livingatlas.arcgis.com/landcover/">https://livingatlas.arcgis.com/landcover/</a> Esri Sentinel-2 Land Cover	10 m × 10 m
Rainfall	<a href="https://www.chc.ucsb.edu/data/chirps">https://www.chc.ucsb.edu/data/chirps</a> CHIRPS Precipitation Dataset	5000 m × 5000 m
Drainage Density	<a href="https://earthexplorer.usgs.gov/">https://earthexplorer.usgs.gov/</a> Derived from SRTM DEM	30 m × 30 m
Distance to River	<a href="https://earthexplorer.usgs.gov/">https://earthexplorer.usgs.gov/</a> Derived from drainage network (SRTM DEM)	30 m × 30 m
Distance to Road	<a href="https://www.openstreetmap.org/">https://www.openstreetmap.org/</a> OpenStreetMap Road Network	30 m × 30 m

## 236 **Modeling and Spatial Cross-Validation**

237 To assess flood susceptibility, eight different classical machine learning models were  
238 implemented, including the Decision Tree, Random Forest, Extra Trees, AdaBoost, Gradient  
239 Boosting, HistGradientBoosting and two very efficient tree ensemble methods, XGBoost and  
240 LightGBM (Arrogante-Funes et al. 2024). Instead of conventional random splitting methods,  
241 this study adopts a blocked spatial cross-validation strategy to tackle the issue of spatial data  
242 leakage stemming from spatial autocorrelation. The study area was split into 10 spatial folds,  
243 with a geographically distinct block of 5000 units from the total number of pixels within this  
244 fold used for validation and testing respectively, while all other folds were used for training.  
245 Such rigid spatial separation guarantees that model evaluation samples do not correlate with  
246 training data in space, avoiding over-optimistic performance estimates and forcing to  
247 generalize relationships between flood occurrence and environmental predictors (Dal Seno et  
248 al. 2024). All the models were trained on data seamless pre-processing pipeline and its  
249 hyperparameter tuning was performed on validation fold to provide a leak free evaluation  
250 framework. Finally, SHAP analysis is employed on some models to interpret feature  
251 contributions and improve model interpretability.

252

$$\text{Accuracy} = \frac{TP + TN}{TP + TN + FP + FN} \quad 2$$

$$\text{Precision} = \frac{TP}{TP + FP} \quad 3$$

$$\text{Recall} = \frac{TP}{TP + FN} \quad 4$$

$$\text{F1} = 2 \cdot \frac{\text{Precision} \cdot \text{Recall}}{\text{Precision} + \text{Recall}} \quad 5$$

253

254

255

256

257

258

259

260

261

262

263

264

265

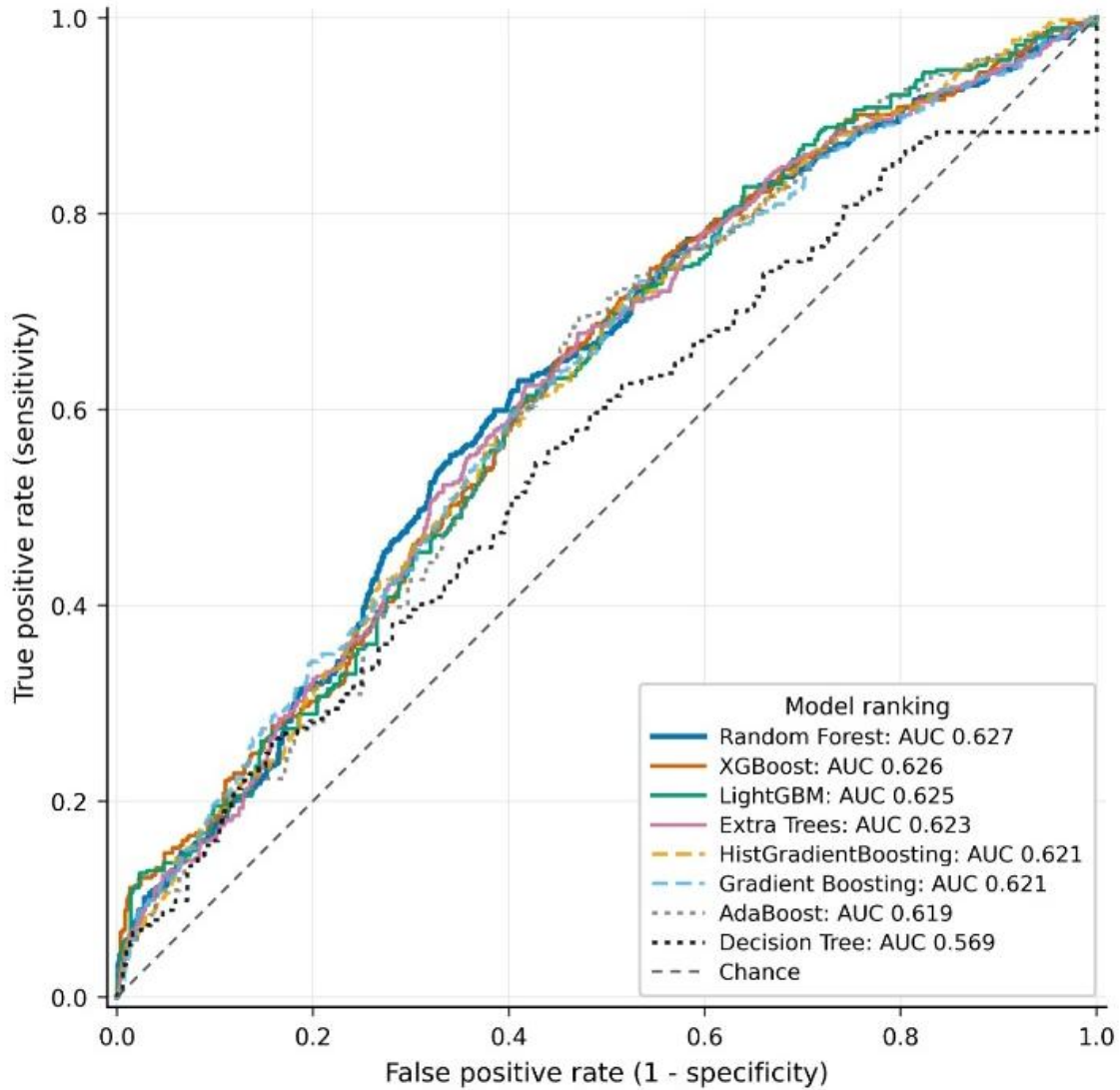
266

267

268 **Results**

269 **Performance Assessment**

270 For continued validation results, it was found that XGBoost (ROC-AUC = 0.6256) performed  
271 best, with LightGBM (0.6254) and Random Forest (0.6270) closely behind.



272

273

Figure 4: ROC-AUC Curves for models

274 Notice that XGBoost also yielded the highest average precision and F1-score (which capture  
275 its ability for modeling nonlinear relationships and handling class-imbalances), the second-  
276 highest ROC-AUC score and lowest root-relative error. Other ensemble models performed just  
277 a bit worse but competitively like HistGradientBoosting and Gradient Boosting.

278

279

280

Table 2: Performance Overview

<i>Model</i>	<i>Family</i>	<i>Roc-Auc</i>	<i>Average Precision</i>	<i>Accuracy</i>	<i>Balanced Accuracy</i>	<i>Precision</i>	<i>Recall</i>	<i>F1</i>	<i>Mcc</i>
<b>Random Forest</b>	Tree Ensemble	0.6270	0.3879	0.6025	0.6014	0.3565	0.5990	0.4470	0.1805
<b>XGBoost</b>	Boosting	0.6256	0.4024	0.5718	0.5989	0.3440	0.6574	0.4516	0.1753
<b>LightGBM</b>	Boosting	0.6254	0.3971	0.6331	0.5684	0.3499	0.4289	0.3854	0.1290
<b>Extra Trees</b>	Tree Ensemble	0.6227	0.3738	0.5977	0.5941	0.3505	0.5863	0.4387	0.1676
<b>HistGradient Boosting</b>	Boosting	0.6208	0.3686	0.6501	0.5624	0.3551	0.3731	0.3639	0.1228
<b>Gradient Boosting</b>	Boosting	0.6207	0.3707	0.5970	0.5856	0.3453	0.5609	0.4275	0.1529
<b>AdaBoost</b>	Boosting	0.6193	0.3749	0.5943	0.5877	0.3456	0.5736	0.4313	0.1564
<b>Decision Tree</b>	Tree	0.5689	0.3410	0.4425	0.5371	0.2894	0.7411	0.4163	0.0708

282 As demonstrated in table 3, ROC-AUC and average precision performance on the test dataset  
 283 indicates that ensemble methods outperform single-tree models across the board; random forest  
 284 leads in ROC-AUC performance while XGBoost leads high precision-recall performance.

285

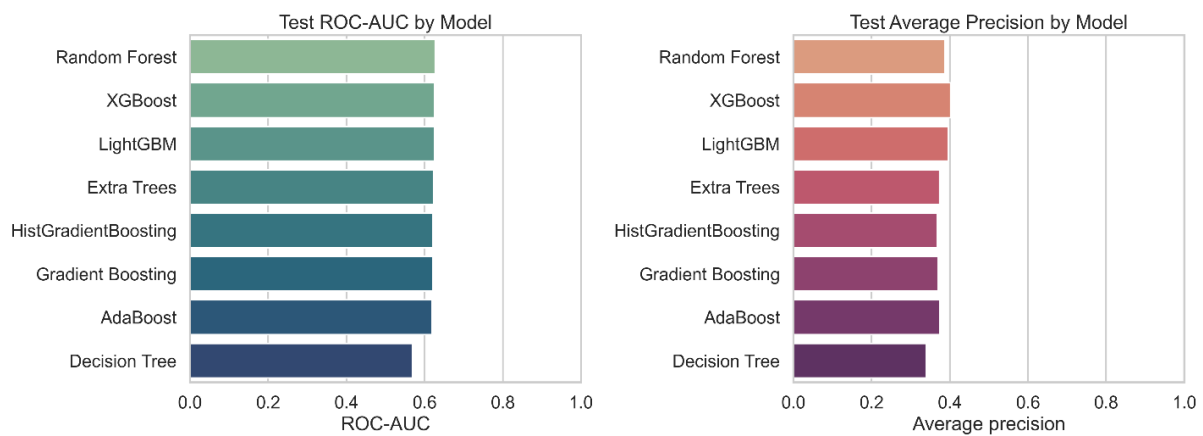


Figure 5: ROC-AUC and Average Precision

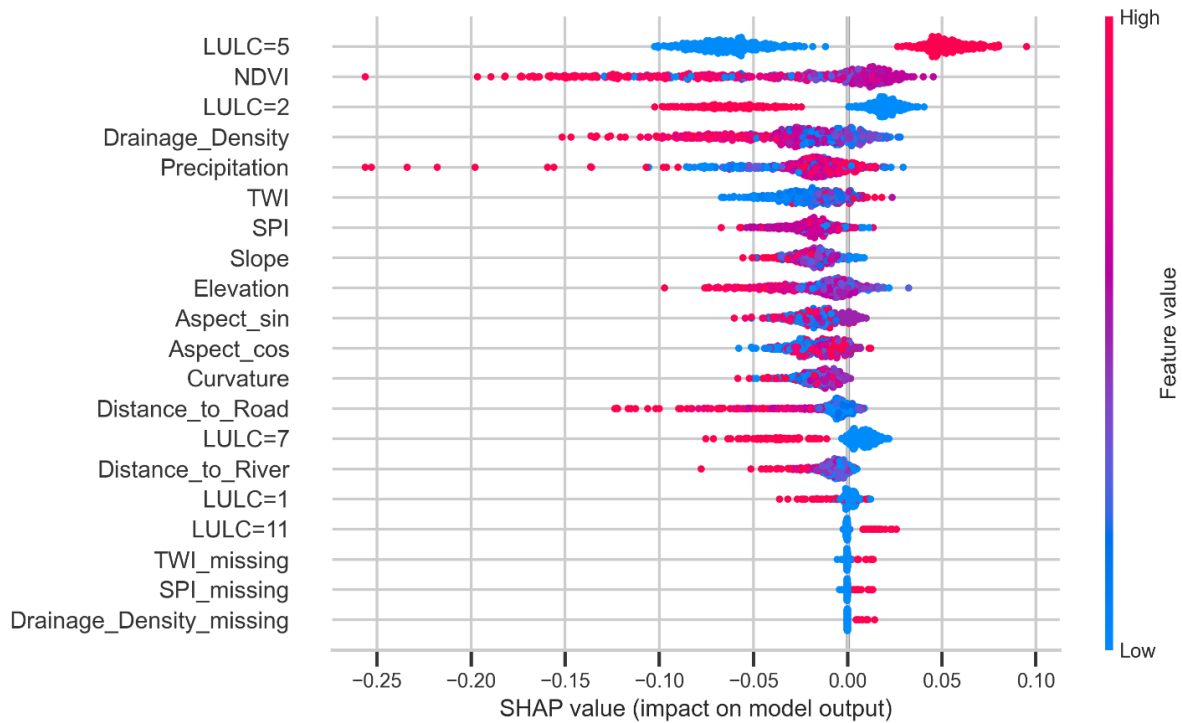
286 In Conclusion Based on Overall Performace Random Forest was chosen as Final Model. While  
 287 XGBoost had higher average precision and F1-score, Random Forest produced better ROC-  
 288 AUC and more consistent generalization under spatial evaluation, making it favorable for  
 289 regional-scale susceptibility mapping.

290

### 291 Model Interpretability (SHAP Analysis)

292 To enhance the interpretability of the selected model, SHAP (SHapley Additive exPlanations)  
 293 analysis was conducted on the Random Forest model to quantify the contribution of individual  
 294 conditioning factors to flood susceptibility predictions. SHAP provides a unified framework

295 for interpreting complex machine learning models by assigning each feature an important value  
 296 based on its marginal contribution to the prediction outcome.



297  
 298

Figure 6: SHAP Result

299 Figure X shows the SHAP summary plot, features are ranked by mean absolute value and the  
 300 distribution of SHAP values indicates both simultaneous impact on flood occurrence  
 301 magnitude & direction. The color gradient (from red to blue) corresponds to feature values:  
 302 higher states are in red and lower states are in blue.

303 These findings suggest that among the most important predictors are Land Use/Land Cover  
 304 (LULC), NDVI and drainage density. Some land-use and land-cover (LULC) classes (e.g.,  
 305 LULC=5 and LULC=2) are positively strong contributors to flood susceptibility, indicating  
 306 that those types of land use likely low-lying agricultural or built-up areas are more susceptible  
 307 to inundation, while others have weak positive contributions or appear to reduce the likelihood  
 308 of inundation.

309 NDVI has been found to be inversely proportional to flood susceptibility: the more vegetation  
 310 cover there is, the lower a location is with respect to susceptible areas to floods; likely maybe  
 311 due more infiltration and less surface run off (Aldiansyah and Wardani 2023).

312 Within the hydrological parameters, the drainage density, precipitation and TWI are prominent.  
 313 The use of these variables indicates an increased susceptibility to flooding, because higher  
 314 values of these variables are associated with a greater accumulation of runoff and more  
 315 effective water retention (Al-Kindi and Alabri 2024).

316 Topographic variables like elevation and slope follow expected patterns where lower elevation  
 317 means higher flood susceptibility and flatter slopes correspond to more flooding risk while  
 318 higher elevation will mean reduced flooding probability, as well as steeper slopes (Hajji et al.  
 319 2025).

320 Predictions are also influenced by distance-based variables such as distance to rivers and roads  
 321 (Yuan et al. 2023). There are more complex effects for road distance, as close proximity to

322 roads actually appears to increase susceptibility even though mere distance from rivers is  
323 correlatively less susceptible and areas immediately adjacent a river show the most relative  
324 vulnerability likely due to localized changes in drainage pathways (Hajji et al. 2025).

325 In summary, the SHAP analysis confirms that the model is indeed able to capture meaningful  
326 relationships of environmental factors regulating flood occurrence capturing complex  
327 interactions between hydrological processes and land-use characteristics that shape flood  
328 proneness in Greater Noakhali.

### 329 Flood Susceptibility Mapping

330 Based on the performance assessment, the Random Forest model was selected to generate the  
331 final flood susceptibility map for the Greater Noakhali region. The model output, initially  
332 obtained as continuous probability values, was reclassified into five susceptibility classes: very  
333 low, low, medium, high and very high to improve readability and guide on-ground decision-  
334 making.

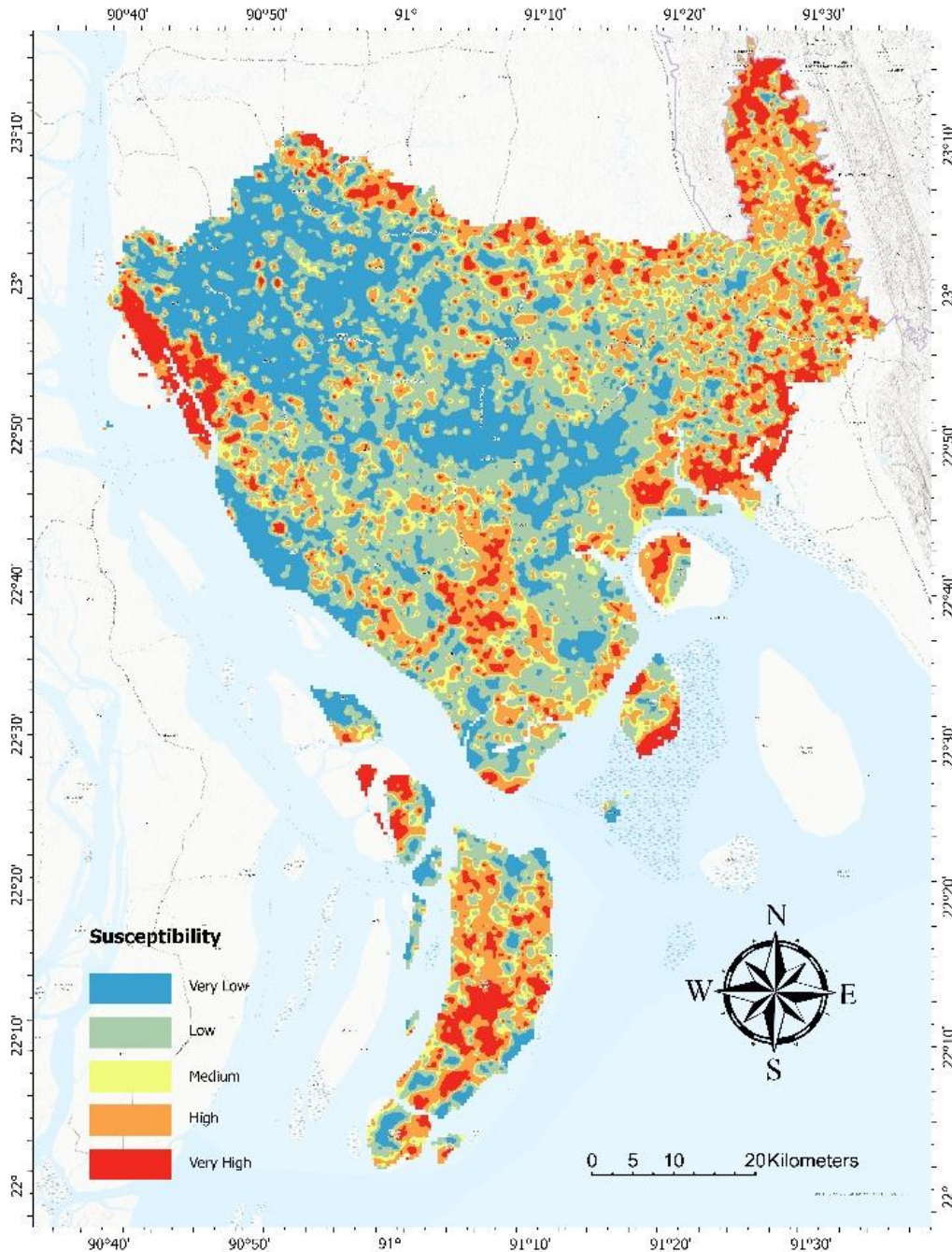
335 In Figure 7, it shows that flood risk is significantly higher in the regions of Meghna estuary  
336 and nearby distributaries due to merging effects of river discharge and tidal effects. Likewise,  
337 areas of high susceptibility inland are also observed in places with high drainage density, low  
338 elevation and land use intensity which carry surface runoff and accumulate within the field.

339 Moderate susceptibility zones are further scattered across transitional landscapes, driven by  
340 minor terrain variation and the domain of extensive land use types that influence localized flood  
341 processes. On the contrary, low and very low susceptibility areas are mostly located within  
342 largely elevated urban regions under better natural drainage condition.

343 The spatial patterns of susceptibility map are consistent with the SHAP analysis result. Crucial  
344 controlling factors (e.g. LULC, NDVI, drainage density and precipitation) exhibit major  
345 dominance in flood-prone zones which validates the physical topology of model output results.  
346 Low NDVI areas and specific land-use types, for example, have the tendency to closely align  
347 with high-susceptibility clusters and regions subjected to higher elevation and slope tend to  
348 correspond well with low-risk zones.

349 Additionally, Random Forest model outputs are spatially coherent and smooth, thus preventing  
350 fragmentation and noise in the surface of predictions. This feature improves the applicability  
351 of the map to regional-scale planning and flood risk management.

352



353  
354

*Figure 7: Flood Susceptibility Map*

355 Overall, the generated flood susceptibility map provides a realistic representation of flood-  
 356 prone areas in the Greater Noakhali region and demonstrates the effectiveness of leakage-aware  
 357 machine learning in capturing spatial flood dynamics. The map can serve as a valuable tool for  
 358 land-use planning, disaster preparedness, and climate adaptation strategies in this highly  
 359 vulnerable coastal region.

## 360 Discussion

361 This study highlights a crucial shift needed in geospatial flood modelling: moving from simple  
 362 "memorization" to more realistic "generalization". Unlike traditional flood susceptibility  
 363 research in Bangladesh, which often reports very high ROC-AUC scores (>0.90) with random  
 364 train-test splits, our findings show more moderate scores (around 0.62–0.63). Although lower

365 in number, these scores offer a more accurate assessment of model performance in areas not  
366 seen during training. Using a blocked spatial cross-validation approach, we reduced bias caused  
367 by spatial autocorrelation, enabling the models to learn true physical relationships rather than  
368 relying on proximity patterns (Vainio et al. 2021). One reason for the moderate scores is that  
369 we considered the dataset imbalanced without creating synthetic data to balance it, because  
370 most cases in the natural hazards dataset are inherently imbalanced (Eltehewy et al. 2023).

371 Among the ensemble architectures, bagging-based Random Forest and boosting-based  
372 XGBoost demonstrated superior stability. While XGBoost excelled in precision and F1 score,  
373 suggesting a high sensitivity to flood-positive pixels, Random Forest was selected for final  
374 mapping due to its superior ROC-AUC (0.6270) and more coherent spatial prediction behavior.  
375 This suggests that while boosting models are adept at capturing complex minority-class  
376 patterns, bagging-based approaches may offer the robustness required for regional-scale hazard  
377 assessment under strict spatial constraints.

378 The SHAP analysis provided a physically interpretable "glass-box" view into these ensemble  
379 models. The dominance of LULC, NDVI, and drainage density highlights the combined  
380 influence of anthropogenic modifications and natural hydrological networks (Bhattarai et al.  
381 2025). Specifically, the strong inverse relationship between NDVI and flood susceptibility  
382 confirms that vegetation cover acts as a natural buffer by enhancing infiltration and slowing  
383 surface runoff. Furthermore, the spatial alignment of high-susceptibility zones with the Meghna  
384 estuary and low-lying coastal tracts confirms the model's ability to capture the dual influence  
385 of fluvial discharge and tidal propagation characteristic of deltaic environments (Jamei et al.  
386 2022).

387 Despite the rigor of the leakage-aware framework, limitations remain. The reliance on a single  
388 flood event (August 2024) and the 30m resolution of the SRTM DEM may omit hyper-local  
389 drainage nuances. Future research should explore multi-temporal inventories and integrate  
390 high-resolution soil moisture data to further refine these predictive surfaces.

## 391 **Conclusion**

392 This study successfully establishes a stringent, leakage-aware machine learning framework for  
393 flood susceptibility mapping in the Greater Noakhali region of Bangladesh. By moving beyond  
394 standard random validation techniques, this research directly addresses the pervasive issue of  
395 spatial data leakage that plagues geospatial modelling, often leading to misleading and over-  
396 optimistic hazard assessments. Our comparative evaluation confirms that tree-based ensemble  
397 models, specifically Random Forest and XGBoost, deliver credible and stable flood-risk  
398 predictions under strict spatial holdout validation in a dynamic deltaic landscape. Integrating  
399 Sentinel-1 SAR imagery with SHAP-based interpretability yielded a transparent methodology  
400 that identified hydrological density, vegetation cover, and land-use patterns as the foremost  
401 drivers of inundation. The resulting susceptibility map accurately delineates critical high-risk  
402 zones concentrated along coastal and riverine corridors, supplying a realistic and operationally  
403 viable decision-support tool for land-use planning and early warning systems. Ultimately, this  
404 research underscores the absolute necessity of adopting spatially robust validation as a  
405 foundational standard for geospatial AI, ensuring the reliability of flood risk interventions and  
406 climate adaptation strategies in highly vulnerable regions.

407

408

409

## 410 **References**

- 411 Abedin J, Rabby YW, Hasan I, Akter H (2020) An investigation of the characteristics, causes,  
412 and consequences of June 13, 2017, landslides in Rangamati District Bangladesh.  
413 *Geoenvironmental Disasters* 7:23. <https://doi.org/10.1186/s40677-020-00161-z>
- 414 Aldiansyah S, Wardani F (2023) Evaluation of flood susceptibility prediction based on a  
415 resampling method using machine learning. *J Water Clim Change* 14:937–961.  
416 <https://doi.org/10.2166/wcc.2023.494>
- 417 Ali M, Amin MdK, Hasan GMJ (2025) Assessing the correlation between sea level rise,  
418 temperature, and erosion-accretion along the coastline of Bangladesh. *Discov Geosci*  
419 3:22. <https://doi.org/10.1007/s44288-025-00129-2>
- 420 Alif HA, Mashrafi MdJ, Elhag M, Purohit S (2025) Artificial Intelligence-Driven Rainfall  
421 Forecasting and GIS-Based Flood Risk Mapping for Climate-Resilient Infrastructure in  
422 Bangladesh. *Earth Syst Environ*. <https://doi.org/10.1007/s41748-025-00958-8>
- 423 Al-Kindi KM, Alabri Z (2024) Investigating the Role of the Key Conditioning Factors in Flood  
424 Susceptibility Mapping Through Machine Learning Approaches. *Earth Syst Environ*  
425 8:63–81. <https://doi.org/10.1007/s41748-023-00369-7>
- 426 Aniramu O, Iyanda O, Orimoogunje O (2026) Remote sensing and GIS-based modelling of  
427 land use dynamics and urban flood risk in Lagos megacity for future flood mitigation.  
428 *Sci Rep* 16:8125. <https://doi.org/10.1038/s41598-026-38544-1>
- 429 Arrogante-Funes P, Bruzón AG, Álvarez-Ripado A, et al (2024) Assessment of the  
430 regeneration of landslides areas using unsupervised and supervised methods and  
431 explainable machine learning models. *Landslides* 21:275–290.  
432 <https://doi.org/10.1007/s10346-023-02154-z>
- 433 Asrade TM, Abebe SA, Tadesse KB, et al (2026) Flood susceptibility assessment using three  
434 machine learning techniques and comparison of their performance. *Sci Rep* 16:8099.  
435 <https://doi.org/10.1038/s41598-026-38391-0>
- 436 Bhattarai Y, Chaudhary V, Walker C, et al (2025) Ensemble learning for enhancing critical  
437 infrastructure resilience to urban flooding. *Sci Rep* 15:36901.  
438 <https://doi.org/10.1038/s41598-025-20970-2>
- 439 Dahim M, Alqadhi S, Mallick J (2023) Enhancing landslide management with hyper-tuned  
440 machine learning and deep learning models: Predicting susceptibility and analyzing  
441 sensitivity and uncertainty. *Front Ecol Evol* 11:.  
442 <https://doi.org/10.3389/fevo.2023.1108924>
- 443 Dal Seno N, Evangelista D, Piccolomini E, Berti M (2024) Comparative analysis of  
444 conventional and machine learning techniques for rainfall threshold evaluation under  
445 complex geological conditions. *Landslides* 21:2893–2911.  
446 <https://doi.org/10.1007/s10346-024-02336-3>
- 447 Das G, Lepcha K (2019) Application of logistic regression (LR) and frequency ratio (FR)  
448 models for landslide susceptibility mapping in Relli Khola river basin of Darjeeling  
449 Himalaya, India. *SN Appl Sci* 1:1453. <https://doi.org/10.1007/s42452-019-1499-8>

- 450 Das S, Hazra S, Haque A, et al (2021) Social vulnerability to environmental hazards in the  
 451 Ganges-Brahmaputra-Meghna delta, India and Bangladesh. *Int J Disaster Risk Reduct*  
 452 53:101983. <https://doi.org/10.1016/j.ijdr.2020.101983>
- 453 Dixit S, Pandey KK, Shukla D (2024) Decadal hydrological impact assessment of evolving  
 454 land use and land cover in an Indian river basin: a multi-model approach. *J Water Clim*  
 455 *Change* 15:4418–4433. <https://doi.org/10.2166/wcc.2024.120>
- 456 Dutta D, Srinivas VV, Bala G (2025) Disparity in spatiotemporal variability and risk of  
 457 compound coastal extremes between India's East-West coasts. *Npj Clim Atmospheric*  
 458 *Sci* 8:168. <https://doi.org/10.1038/s41612-025-01045-5>
- 459 Elahi MWE, Wang XH, Ritchie EA (2025) Cyclone-induced storm surge flooding in the  
 460 Ganges-Brahmaputra-Meghna delta under different mean-sea level rise scenarios.  
 461 *Ocean Dyn* 75:27. <https://doi.org/10.1007/s10236-025-01671-w>
- 462 Elmotawakkil A, Moumane A, Zahi A, et al (2025) HydroPredictor a hybrid machine learning  
 463 model for addressing data scarcity in groundwater prediction. *Sci Rep* 15:44069.  
 464 <https://doi.org/10.1038/s41598-025-24960-2>
- 465 Eltehewy R, Abouelfarag A, Saleh SN (2023) Efficient Classification of Imbalanced Natural  
 466 Disasters Data Using Generative Adversarial Networks for Data Augmentation. *ISPRS*  
 467 *Int J Geo-Inf* 12:245. <https://doi.org/10.3390/ijgi12060245>
- 468 Ganiyu HO, Jaafar WZW, Othman F, Ng CY (2026) Enhancing flood simulation in data-sparse  
 469 Niger central hydrological area river basin in Nigeria using machine learning-based  
 470 data fusion. *Theor Appl Climatol* 157:204. [https://doi.org/10.1007/s00704-026-06091-](https://doi.org/10.1007/s00704-026-06091-4)  
 471 4
- 472 Ghasemian B, Shahabi H, Shirzadi A, et al (2022) A Robust Deep-Learning Model for  
 473 Landslide Susceptibility Mapping: A Case Study of Kurdistan Province, Iran. *Sensors*  
 474 22:1573–1573. <https://doi.org/10.3390/s22041573>
- 475 Grekousis G (2025) Geographical-XGBoost: a new ensemble model for spatially local  
 476 regression based on gradient-boosted trees. *J Geogr Syst* 27:169–195.  
 477 <https://doi.org/10.1007/s10109-025-00465-4>
- 478 Gupta R, Gambhir S, Krejcar O, et al (2026) Data-driven explainable chronic kidney disease  
 479 detection using RF based data imputation and meta-ensemble learning. *Sci Rep*  
 480 16:12679. <https://doi.org/10.1038/s41598-026-41425-2>
- 481 Habumugisha JM, Chen N, Rahman M, et al (2022) Landslide Susceptibility Mapping with  
 482 Deep Learning Algorithms. *Sustainability* 14:1734.  
 483 <https://doi.org/10.3390/su14031734>
- 484 Hajji S, Krimissa S, Abdelrahman K, et al (2025) Enhancing flood prediction through remote  
 485 sensing, machine learning, and Google Earth Engine. *Front Water* 7:.  
 486 <https://doi.org/10.3389/frwa.2025.1514047>
- 487 Huang P-C (2025) Performance Evaluation of a Substituted Topography-based Model To  
 488 Forecast Rainfall and tide-induced Lowland Flooding. *Water Resour Manag* 39:7201–  
 489 7226. <https://doi.org/10.1007/s11269-025-04293-5>

- 490 Hussain MA, Chen Z, Zheng Y, et al (2023) Deep Learning and Machine Learning Models for  
 491 Landslide Susceptibility Mapping with Remote Sensing Data. *Remote Sens* 15:4703.  
 492 <https://doi.org/10.3390/rs15194703>
- 493 Islam ARMdT, Mamun MdA-A, Tasnuva A, et al (2026) Living on the flood line: Constructing  
 494 and validating a combined multidimensional resilience index for rural riverine  
 495 floodplain communities. *Sci Total Environ* 1020:181581.  
 496 <https://doi.org/10.1016/j.scitotenv.2026.181581>
- 497 Jamei M, Karbasi M, Malik A, et al (2022) Computational assessment of groundwater salinity  
 498 distribution within coastal multi-aquifers of Bangladesh. *Sci Rep* 12:11165.  
 499 <https://doi.org/10.1038/s41598-022-15104-x>
- 500 Khan MJU (2021) Dynamics of inundation events in the rivers-estuaries-ocean continuum in  
 501 Bengal delta : synergy between hydrodynamic modelling and spaceborne remote  
 502 sensing. Theses, Université Paul Sabatier - Toulouse III
- 503 Kumar A, Pandey G, Kale RV (2026) Ensemble machine learning and deep learning  
 504 framework for flood susceptibility mapping in the transboundary Rapti River Basin.  
 505 *Environ Earth Sci* 85:168. <https://doi.org/10.1007/s12665-026-12912-6>
- 506 Li D, Gajardo J, Volpi M, Defraeye T (2023) Using machine learning to generate an open-  
 507 access cropland map from satellite images time series in the Indian Himalayan region.  
 508 *Remote Sens Appl Soc Environ* 32:101057.  
 509 <https://doi.org/10.1016/j.rsase.2023.101057>
- 510 Murad G, Nawar N, Ashrafi H, et al (2025) Comprehensive Landslide Inventory and Hotspot  
 511 Analysis in the Chittagong Hill Tracts of Southeastern Bangladesh. In: *Proceedings of*  
 512 *International Conference on Civil Engineering Research & Innovations*
- 513 Murad G, Rahman MA, Srabony SC, Mahmud S (2026) Uncertainty-Aware Bayesian Machine  
 514 Learning for Landslide Susceptibility Mapping: in the Chattogram Metropolitan Hill  
 515 System, Bangladesh
- 516 Nnam VC, Odumosu JO, Uche I, Lamidi S (2026) Deep learning-enhanced shoreline dynamics  
 517 and vulnerability assessment in Niger Delta area of Nigeria. *Sci Rep* 16:12595.  
 518 <https://doi.org/10.1038/s41598-026-39405-7>
- 519 Paszkowski A, Tiggeloven T, Borgomeo E, Hall JW (2025) Disparities in exposure to  
 520 hydrogeomorphic hazards in Bangladesh. *Nat Commun* 16:10208.  
 521 <https://doi.org/10.1038/s41467-025-64920-y>
- 522 Piya FA, Evan SJ, Rahman MdM, Tabassum A (2026) Flood susceptibility mapping using  
 523 multiple multi-criteria decision-making methods, Gaibandha district of northern  
 524 Bangladesh. *Discov Geosci* 4:116. <https://doi.org/10.1007/s44288-026-00491-9>
- 525 Rahimi M, Malekmohammadi B, Firozjaei MK, et al (2026) Integrating geospatial intelligence  
 526 and machine learning for flood susceptibility mapping. *Sci Rep* 16:10228.  
 527 <https://doi.org/10.1038/s41598-026-41014-3>

- 528 Rahman M, Yasuhara H (2026) SPATIAL SPARSITY AWARE EXPLAINABLE DEEP  
529 LEARNING-BASED LANDSLIDE SUSCEPTIBILITY MAPPING: APPLICATION  
530 TO A HILL DISTRICT, BANGLADESH
- 531 Rashid M, Ullah S, Farnaz, et al (2026) Integrated Data-Driven Multi-Criteria Analysis and  
532 Machine Learning Approaches for Assessment of Flood Susceptibility Mapping. *Water*  
533 18:844. <https://doi.org/10.3390/w18070844>
- 534 Ren T, Gao L, Gong W (2024) An ensemble of dynamic rainfall index and machine learning  
535 method for spatiotemporal landslide susceptibility modeling. *Landslides* 21:257–273.  
536 <https://doi.org/10.1007/s10346-023-02152-1>
- 537 Sarker S, Jahan I (2026) Strengthening flash flood resilience in coastal Bangladesh through  
538 vulnerability drivers and policy reform. *Discov Hazards* 2:4.  
539 <https://doi.org/10.1007/s44475-026-00009-4>
- 540 Shampa, Nasir NN, Winey MM, et al (2025) Integration of Remote Sensing and Machine  
541 Learning Approaches for Operational Flood Monitoring Along the Coastlines of  
542 Bangladesh Under Extreme Weather Events. *Water* 17:2189.  
543 <https://doi.org/10.3390/w17152189>
- 544 Shatov V, Schieler S, Muth C, et al (2026) Integrated Radio Sensing Capabilities for 6G  
545 Networks: AI/ML Perspective. *IEEE Commun Surv Tutor* 28:5081–5120.  
546 <https://doi.org/10.1109/COMST.2026.3668458>
- 547 Sorna UN, Saif SB, Islam FAS (2025) Modeling Relative Sea-Level Rise through Geodetic-  
548 Hydrodynamic Fusion: Quantifying Multi-Sectoral Risks in the Bengal Delta. *Int J*  
549 *Appl Nat Sci* 3:29–66. <https://doi.org/10.61424/ijans.v3i3.541>
- 550 Tella A, Pham QB, Zahidi I, et al (2026) Advancing Flood Susceptibility Mapping with  
551 Explainable AI: A Novel Application of Accumulated Local Effects (ALE). *Water*  
552 *Resour Manag* 40:140. <https://doi.org/10.1007/s11269-025-04430-0>
- 553 Vainio E, Peltola O, Kasurinen V, et al (2021) Topography-based statistical modelling reveals  
554 high spatial variability and seasonal emission patches in forest floor methane flux.  
555 *Biogeosciences* 18:2003–2025. <https://doi.org/10.5194/bg-18-2003-2021>
- 556 Valentine LA, Wilson CA (2023) Riverbank erosion and char stability along the fluvial-to-tidal  
557 transition zone in the Lower Meghna River and Tentulia Channel in the Ganges-  
558 Brahmaputra-Meghna Delta, Bangladesh. *Geomorphology* 432:108692.  
559 <https://doi.org/10.1016/j.geomorph.2023.108692>
- 560 Yao J, Zhao Z, Pan M, et al (2026) SWOT-based water surface elevation observations improve  
561 flood modeling of the 25·7 Miyun reservoir basin extreme rainfall event. *Npj Nat*  
562 *Hazards* 3:12. <https://doi.org/10.1038/s44304-026-00176-w>
- 563 Yuan F, Lee C-C, Mobley W, et al (2023) Predicting road flooding risk with crowdsourced  
564 reports and fine-grained traffic data. *Comput Urban Sci* 3:15.  
565 <https://doi.org/10.1007/s43762-023-00082-1>
- 566